Originals

Computational Mechanics 19 (1996) 120 - 135 © Springer-Verlag 1996

Admissible approximations for essential boundary conditions in the reproducing kernel particle method

J. Gosz, W. K. Liu

Abstract In the reproducing kernel particle method (RKPM), and meshless methods in general, enforcement of essential boundary conditions is awkward as the approximations do not satisfy the Kronecker delta condition and are not admissible in the Galerkin formulation as they fail to vanish at essential boundaries. Typically, Lagrange multipliers, modified variational principles, or a coupling procedure with finite elements have been used to circumvent these shortcomings.

Two methods of generating admissible meshless approximations, are presented; one in which the RKPM correction function equals zero at the boundary, and another in which the domain of the window function is selected such that the approximate vanishes at the boundary. An extension of the RKPM dilation parameter is also introduced, providing the capability to generate approximations with arbitrarily shaped supports. This feature is particularly useful for generating approximations near boundaries that conform to the geometry of the boundary. Additional issues such as degeneration of shape functions from 2D to 1D and moment matrix conditioning are also addressed.

1 Introduction

In applying the Galerkin method to meshless methods such as the reproducing kernel particle method (RKPM) (Liu, Chen, Jun, Chen, Belytschko, Pan, Uras, and Chang, 1996; Liu, Chen, Chang, and Belytschko, 1996; Liu and Chen, 1995; Liu, Jun, Li, Adee, and Belytschko, 1995; Liu, Jun, and Zhang, 1995), difficulties arise because the approximates or shape functions generally do not satisfy the Kronecker delta condition. Furthermore, the approximates are not guaranteed to vanish at boundaries where essential boundary conditions are prescribed.

Many solutions to this problem have been proposed for the various meshless methods. For example the element free Galerkin method (EFG) has incorporated Lagrange multipliers (Belytschko, Lu, and Gu, 1994), modified variational principles (Lu, Belytschko, and Gu, 1994), and a coupling procedure with the finite element method (Krongauz and Belytschko, 1996). The h-p cloud method has implemented Lagrange multipliers and has also reported that a method which incorporates singular weighting functions in Galerkin method format shows promise (Duarte and Oden, 1995). The finite point method (FPM) advocates point-wise enforcement of essential boundaries (Oñate, Idelsohn, Zienkiewicz, Taylor, and Sacco, 1996). Other proposed methods include penalty methods, collocation, and perturbed Lagrangian.

While these methods provide a means of overcoming the inherent difficulties of meshless methods, none has yet provided an inclusive method of conveniently handling boundaries with essential conditions. Furthermore, each method has limitations and drawbacks. For example, Lagrange multipliers pose difficulties in that the resulting stiffness matrix is no longer positive definite or banded, and the size of the problem is increased. While modified variational principles enable the stiffness matrix to remain positive definite and banded, they are reported to be less accurate and are rather inconvenient. Coupling with finite elements negates some of the advantages of meshless approximates and can result in discontinuities in the derivatives of the approximates.

In the finite element method, essential boundary conditions are efficiently enforced because the shape functions of nodes not lying on the essential boundary automatically vanish at the boundary. Furthermore, the FEM approximations possess the Kronecker delta property. As a result a zero displacement boundary condition, for example, can be easily satisfied by setting the nodal values of nodes lying on the boundary to zero. A positive definite stiffness matrix results and the size of the problem is actually reduced. This method of enforcing essential boundary conditions has proved very convenient and intuitive.

At this point it is not realistic to think that the classical method of handling essential boundaries in the finite element method can be fully extended to meshless methods, however, there is evidence that a similar approach can be used successfully on a number of important boundaries (Liu, Li, and Belytschko, 1996). Specifically, by utilizing the flexibility of the meshless shape functions, the shape functions can be enforced to vanish at essential boundaries. In RKPM it can be seen by the definition of the shape function

$$N_j(\mathbf{x}) = C(\mathbf{x}; \mathbf{x} - \mathbf{x}_j)\phi_{a_j}(\mathbf{x} - \mathbf{x}_j)\Delta V_j$$

Communicated by S. N. Atluri, 2 August 1996

J. Gosz, W. K. Liu
Department of Mechanical Engineering, Northwestern University, 2145 Sheridan Road, Evanston, IL 60208, USA

Correspondence to: W. K. Liu

The support of this research by the Office of Naval Research (ONR) to Northwestern University is gratefully acknowledged.

that if either the correction function, $C(\mathbf{x};\mathbf{x}-\mathbf{x}_j)$, or the window function, $\phi_{a_j}(\mathbf{x}-\mathbf{x}_j)$, equals zero at the boundary, the shape function itself will equal zero. By utilizing this concept and by introducing an extension of the dilation parameter termed a dilation function, $a_j(\mathbf{x})$, shape functions in the vicinity of an essential boundary condition can be made to conform to the boundary and vanish at the boundary.

The organization of the paper is as follows. Section 2 provides a brief review of the reproducing kernel particle method while Section 3 incorporates the new concept of a dilation function. The (Bubnov-) Galerkin Method is described in the context of meshless methods in Section 4. Section 5 is a study of admissible approximations near essential boundaries and is followed by numerical examples in Section 6. Conclusions are given in Section 7.

2
Review of the reproducing kernel particle method (RKPM)

The purpose of this section is to review the main features of the reproducing kernel particle method and present it in a format that can be readily implemented. A body Ω in $\mathcal{R}^2$ will be considered with independent variables $\mathbf{x}$, where $\mathbf{x}^{\mathrm{T}}=[x_1,x_2]$.

The mathematical foundation of the method is a continuous convolution defined to be the reproducing equation

$$u^{R_a}(\mathbf{x}) = \int_{\Omega_y} u(\mathbf{y})\phi_{\mathrm{a(y)}}(\mathbf{x}-\mathbf{y})\,\mathrm{d}\Omega_y \ . \tag{2.1}$$

Here $u^{R_a}(\mathbf{x})$ is a reproduced function of the original function, $u(\mathbf{y})$, operated on a projector or window, $\phi_{\mathrm{a(y)}}(\mathbf{x}-\mathbf{y})$. In solving partial differential equations, the reproducing kernel particle method solves a weak form of the problem incorporating the Galerkin method. In order to more accurately solve problems of finite domains, Liu (Liu, Jun, and Zhang, 1995) introduced a correction function which modifies the window to maintain completeness near boundaries.

2.1
Reproducing conditions

The underlying motivation of RKPM is to represent a given function exactly up to a specified polynomial order over the entire domain. For linear reproducing conditions $u(\mathbf{y})$ of the continuous convolution is approximated with a first order accurate Taylor series expansion about $\mathbf{x}$.

$$\begin{aligned} u(\mathbf{y}) \cong\ & u(\mathbf{x}) - [(x_1-y_1)u_{,x_1}(\mathbf{x}) \\ & +(x_2-y_2)u_{,x_2}(\mathbf{x})] \ . \end{aligned} \tag{2.2}$$

The expansion is then substituted into Eq. (2.1) yielding

$$\begin{aligned} u^{R_a}(\mathbf{x}) \cong\ & u(\mathbf{x})\int_{\Omega_y}\phi_{a(\mathrm{y})}(\mathbf{x}-\mathbf{y})\mathrm{d}\Omega_y \\ & - u_{,x_1}(\mathbf{x})\int_{\Omega_y}(x_1-y_1)\phi_{a(\mathrm{y})}(\mathbf{x}-\mathbf{y})\mathrm{d}\Omega_y \\ & - u_{,x_2}(\mathbf{x})\int_{\Omega_y}(x_2-y_2)\phi_{a(\mathrm{y})}(\mathbf{x}-\mathbf{y})\mathrm{d}\Omega_y \ . \end{aligned} \tag{2.3}$$

The integrals in Eq. (2.3) can be used to define moments of the window function.

$$m_{00}(\mathbf{a},\mathbf{x}) = \int_{\Omega_y}\phi_{a(\mathrm{y})}(\mathbf{x}-\mathbf{y})\mathrm{d}\Omega_y \tag{2.4a}$$

$$m_{10}(\mathbf{a},\mathbf{x}) = \int_{\Omega_y}(x_1-y_1)\phi_{a(\mathrm{y})}(\mathbf{x}-\mathbf{y})\mathrm{d}\Omega_y \tag{2.4b}$$

$$m_{01}(\mathbf{a},\mathbf{x}) = \int_{\Omega_y}(x_2-y_2)\phi_{a(\mathrm{y})}(\mathbf{x}-\mathbf{y})\mathrm{d}\Omega_y \tag{2.4c}$$

In general the moments are defined as,

$$\begin{aligned} m_{ij}(\mathbf{a},\mathbf{x}) = & \int_{\Omega_y}(x_1-y_1)^i(x_2-y_2)^j \\ & \times\phi_{a(\mathrm{y})}(\mathbf{x}-\mathbf{y})\mathrm{d}\Omega_y \ . \end{aligned} \tag{2.5}$$

Rewriting Eq. (2.3) using the moment definitions (2.4) gives

$$\begin{aligned} u^{R_a}(\mathbf{x}) \cong\ & u(\mathbf{x})m_{00}(\mathbf{a},\mathbf{x}) - u_{,x_1}(\mathbf{x})m_{10}(\mathbf{a},\mathbf{x}) \\ & - u_{,x_2}(\mathbf{x})m_{01}(\mathbf{a},\mathbf{x}) \ . \end{aligned} \tag{2.6}$$

In order for the approximated function to be reproduced exactly, the following reproducing conditons need to be satisfied.

$$m_{00}(\mathbf{a},\mathbf{x}) = 1 \tag{2.7a}$$

$$m_{10}(\mathbf{a},\mathbf{x}) = 0 \tag{2.7b}$$

$$m_{01}(\mathbf{a},\mathbf{x}) = 0 \tag{2.7c}$$

$$\text{or } m_{ij}(\mathbf{a},\mathbf{x}) = \delta_{0i}\delta_{0j} \ . \tag{2.8}$$

An arbitrarily chosen window function does not necessarily satisfy these reproducing conditions. Therefore a corrected window function is obtained by modifying the original window with a polynomial correction function, $C(\mathbf{x};\mathbf{x}-\mathbf{y})$, such that the reproducing conditions are satisfied. The definition used in this approach is

$$\begin{aligned} \bar{\phi}_{\mathrm{a(y)}}(\mathbf{x}-\mathbf{y}) &= C(\mathbf{x};\mathbf{x}-\mathbf{y})\phi_{\mathrm{a(y)}}(\mathbf{x}-\mathbf{y}) \\ &= [b_{00}(\mathbf{a},\mathbf{x}) + b_{10}(\mathbf{a},\mathbf{x})(x_1-y_1) \\ &\quad + b_{01}(\mathbf{a},\mathbf{x})(x_2-y_2)]\phi_{\mathrm{a(y)}}(\mathbf{x}-\mathbf{y}) \\ &= \mathbf{P}^T(\mathbf{x}-\mathbf{y})\mathbf{b}(\mathbf{a},\mathbf{x})\phi_{\mathrm{a(y)}}(\mathbf{x}-\mathbf{y}) \ , \end{aligned} \tag{2.9}$$

with

$$\mathbf{P}(\mathbf{x}-\mathbf{y}) = \begin{bmatrix} 1 \\ (x_1-y_1) \\ (x_2-y_2) \end{bmatrix} \quad \text{and}$$

$$\mathbf{b}(\mathbf{a},\mathbf{x}) = \begin{bmatrix} b_{00}(\mathbf{a},\mathbf{x}) \\ b_{10}(\mathbf{a},\mathbf{x}) \\ b_{01}(\mathbf{a},\mathbf{x}) \end{bmatrix} \ .$$

To calculate the correction coefficients, $\mathbf{b}(\mathbf{a},\mathbf{x})$, the reproducing conditions are applied to the corrected window function. By definition (2.9), the moments of the corrected window function are:

$$\bar{m}_{ij}(\mathbf{a},\mathbf{x}) = \int_{\Omega_y} (x_1 - y_1)^i (x_2 - y_2)^j \times \bar{\phi}_{a(\mathrm{y})}(\mathbf{x}-\mathbf{y})\mathrm{d}\Omega_y \qquad (2.10)$$

From the above definitions, a moment matrix can be defined as

$$\mathbf{M}(\mathbf{a},\mathbf{x}) = \int_{\Omega_y} \mathbf{P}(\mathbf{x}-\mathbf{y})\,\mathbf{P}^T(\mathbf{x}-\mathbf{y}) \times \phi_{a(\mathrm{y})}(\mathbf{x}-\mathbf{y})\mathrm{d}\Omega_y \ . \qquad (2.11)$$

By expanding the moment matrix, it is easily seen that the correction coefficients are obtained via the following linear algebraic system of equations satisfying the reproducing conditions

$$\begin{bmatrix} \bar{m}_{00}(\mathbf{a},\mathbf{x}) \\ \bar{m}_{10}(\mathbf{a},\mathbf{x}) \\ \bar{m}_{01}(\mathbf{a},\mathbf{x}) \end{bmatrix} = \begin{bmatrix} m_{00}(\mathbf{a},\mathbf{x}) & m_{10}(\mathbf{a},\mathbf{x}) & m_{01}(\mathbf{a},\mathbf{x}) \\ & m_{20}(\mathbf{a},\mathbf{x}) & m_{11}(\mathbf{a},\mathbf{x}) \\ symmetric & & m_{02}(\mathbf{a},\mathbf{x}) \end{bmatrix} \begin{bmatrix} b_{00}(\mathbf{a},\mathbf{x}) \\ b_{10}(\mathbf{a},\mathbf{x}) \\ b_{01}(\mathbf{a},\mathbf{x}) \end{bmatrix} = \begin{bmatrix} 1 \\ 0 \\ 0 \end{bmatrix} \quad \text{or} \qquad (2.12)$$

$$\bar{\mathbf{m}}(\mathbf{a},\mathbf{x}) = \mathbf{M}(\mathbf{a},\mathbf{x})\mathbf{b}(\mathbf{a},\mathbf{x}) = \mathbf{P}(\mathbf{0}) \ ,$$

where $\mathbf{P}^T(\mathbf{0}) = [1\ 0\ 0]$. The correction coefficients are thus defined by the following relation

$$\mathbf{b}(\mathbf{a},\mathbf{x}) = \mathbf{M}(\mathbf{a},\mathbf{x})^{-1}\mathbf{P}(\mathbf{0}) \ . \qquad (2.13)$$

2.2
First derivative reproducing conditions

The first derivative of the reproducing equation, Eq. (2.1), with corrected window is defined by

$$\frac{\mathrm{d}}{\mathrm{dx}} u^{Ra}(\mathbf{x}) = \int_{\Omega_y} u(\mathbf{y}) \frac{\mathrm{d}}{\mathrm{dx}} (\bar{\phi}_{\mathrm{a(y)}}(\mathbf{x}-\mathbf{y}))\mathrm{d}\Omega_y \ . \qquad (2.14)$$

Expanding $u(\mathbf{y})$ in a first order accurate Taylor series, as was done for the reproduced function, and representing the integral expressions with moments of the derivatives of the corrected window function, $\bar{m}_{ij,\mathbf{x}}$, Eq. (2.14) can be represented as

$$\frac{\mathrm{d}}{\mathrm{dx}} u^{Ra}(\mathbf{x}) \cong u(\mathbf{x})\bar{m}_{00,\mathbf{x}}(\mathbf{a},\mathbf{x}) - u_{,x_1}(\mathbf{X})\bar{m}_{10,\mathbf{x}}(\mathbf{a},\mathbf{x}) - u_{,x_2}(\mathbf{x})\bar{m}_{0,1,\mathbf{x}}(\mathbf{a},\mathbf{x}) \ , \qquad (2.15)$$

where

$$\bar{m}_{00,\mathbf{x}}(\mathbf{a},\mathbf{x}) = \int_{\Omega_y} \frac{\mathrm{d}}{\mathrm{dx}} (\bar{\phi}_{a(\mathrm{y})}(\mathbf{x}-\mathbf{y}))\mathrm{d}\Omega_y \qquad (2.16a)$$

$$\bar{m}_{10,\mathbf{x}}(\mathbf{a},\mathbf{x}) = \int_{\Omega_y} (x_1 - y_1) \times \frac{\mathrm{d}}{\mathrm{dx}} (\bar{\phi}_{a(\mathrm{y})}(\mathbf{x}-\mathbf{y}))\mathrm{d}\Omega_y \qquad (2.16b)$$

$$\bar{m}_{01,\mathbf{x}}(\mathbf{a},\mathbf{x}) = \int_{\Omega_y} (x_2 - y_2) \frac{\mathrm{d}}{\mathrm{dx}} (\bar{\phi}_{a(\mathrm{y})}(\mathbf{x}-\mathbf{y}))\mathrm{d}\Omega_y \ . \qquad (2.16c)$$

In order to approximate $u^{R_a}_{,x_1}(\mathbf{x})$ and $u^{R_a}_{,x_2}(\mathbf{x})$, definitions (2.16) must be constrained such that the following reproducing conditions are satisfied

$$\bar{m}_{ij,x_1} = -\delta_{1i}\delta_{oj} \quad \text{for } u^{R_a}_{,x_1}(\mathbf{x}) \ , \qquad (2.17)$$

and

$$\bar{m}_{ij,x_2} = -\delta_{0i}\delta_{2j} \quad \text{for } u^{R_a}_{,x_2}(\mathbf{x}) \ . \qquad (2.18)$$

In general, 2D reproducing conditions for the γth derivative are

$$\bar{m}_{ij,\gamma_1\gamma_2} = (-1)^{i+j} i!j!\delta_{i\gamma_1}\delta_{j\gamma_2} \ , \qquad (2.19)$$

where γ_1 represents the order of the partial derivative with respect to x_1, and γ_2 represents the order of the partial derivative with respect to x_2.

Expressing the moments of the corrected window derivatives, $\bar{m}_{ij,\mathbf{x}}$, in terms of moment derivatives of the uncorrected window, $m_{ij,\mathbf{x}}$, correction coefficients and their derivatives yields a system of equations which can be used to derive the correction coefficient derivatives. For example the following relation is obtained for the the derivative with respect to x_1 subject to the above derivative reproducing conditions

$$\begin{bmatrix} m_{00,x_1} & m_{10,x_1} & m_{01,x_1} & m_{00} & m_{10} & m_{01} \\ m_{10,x_1} - m_{00} & m_{20,x_1} - m_{10} & m_{11,x_1} - m_{01} & m_{10} & m_{20} & m_{11} \\ m_{01,x_1} & m_{11,x_1} & m_{02,x_1} & m_{01} & m_{11} & m_{02} \end{bmatrix} \begin{bmatrix} b_{00} \\ b_{10} \\ b_{01} \\ b_{00,x_1} \\ b_{10,x_1} \\ b_{01,x_1} \end{bmatrix} = \begin{bmatrix} 0 \\ -1 \\ 0 \end{bmatrix} \ . \qquad (2.20)$$

By incorporating the reproducing conditions of Eqs. (2.7) into Eq. 2.20, the following simplification results

$$\begin{bmatrix} m_{00,x_1} & m_{10,x_1} & m_{01,x_1} & m_{00} & m_{10} & m_{01} \\ m_{10,x_1} & m_{20,x_1} & m_{11,x_1} & m_{10} & m_{20} & m_{11} \\ m_{01,x_1} & m_{11,x_1} & m_{02,x_1} & m_{01} & m_{11} & m_{02} \end{bmatrix} \begin{bmatrix} b_{00} \\ b_{10} \\ b_{01} \\ b_{00,x_1} \\ b_{10,x_1} \\ b_{01,x_1} \end{bmatrix} = \begin{bmatrix} 0 \\ 0 \\ 0 \end{bmatrix} \ . \qquad (2.21)$$

This result is equivalent to the derivative of Eq. (2.12)

$$\mathbf{M}(\mathbf{a},\mathbf{x})\mathbf{b}(\mathbf{a},\mathbf{x}) = \mathbf{P}(\mathbf{0}) \ ,$$

which is

$$\mathbf{M}_{,\mathbf{x}}(\mathbf{a},\mathbf{x})\mathbf{b}(\mathbf{a},\mathbf{x}) + \mathbf{M}(\mathbf{a},\mathbf{x})\mathbf{b}_{,\mathbf{x}}(\mathbf{a},\mathbf{x}) = \mathbf{0} \ .$$

Thus the derivatives of the correction coefficients can be expressed as

$$\mathbf{b}_{,\mathbf{x}}(\mathbf{a},\mathbf{x}) = -\mathbf{M}^{-1}(\mathbf{a},\mathbf{x})\mathbf{M}_{,\mathbf{x}}(\mathbf{a},\mathbf{x})\mathbf{b}(\mathbf{a},\mathbf{x}) \ .$$

This formulation has been termed the fast derivative computation (Belytschko, Krongauz, Fleming, Organ, and Liu, 1996).

2.3 Discretization

For problems in computational mechanics the convolution equation (2.1) is discretized with trapezoidal rules and represented as

$$u^{R_h}(\mathbf{x}) = \sum_{j=1}^{NP} u(\mathbf{x}_j)\phi_{a_j}(\mathbf{x}-\mathbf{x}_j)\Delta V_j \ , \tag{2.22}$$

where NP is the number of particles and the subscript h is associated with a discretized domain.

While the reproducing conditions have been presented in a continuous case, in implementation the equations are also discretized. To ensure that the sum of the shape functions, $N_j(\mathbf{x})$, equal one over the entire domain, the same integration rule used to discretize the reproducing equation must be used for the moments and their derivatives. The discrete moments using trapezoidal integration are thus defined as

$$\begin{aligned}\tilde{m}_{ij}(\mathbf{a},\mathbf{x}) = &\sum_k (x-x_k)^i (y-y_k)^j \\ &\times \phi_{a_k}(\mathbf{x}-\mathbf{x}_k)\Delta V_k \ .\end{aligned} \tag{2.23}$$

Note that the discrete moment matrix $\tilde{\mathbf{M}}(\mathbf{a},\mathbf{x})$ is non-singular provided there is an admissible particle distribution. For conditions governing an admissible particle distribution refer to (Liu, Li, and Belytschko, 1996).

2.4 Shape functions

The reproducing equations, Eq. (2.22), can be expressed in terms of global shape functions in the usual manner as

$$u^{R_h}(\mathbf{x}) = \sum_{j=1}^{NP} N_j(\mathbf{x})u(\mathbf{x}_j) \ , \tag{2.24}$$

where the global shape functions are defined to be

$$\begin{aligned}N_j(\mathbf{x}) &= \bar{\phi}_{\mathbf{a}_j}(\mathbf{x}-\mathbf{x}_j)\Delta V_j \\ &= C(\mathbf{x};\mathbf{x}-\mathbf{x}_j)\phi_{\mathbf{a}_j}(\mathbf{x}-\mathbf{x}_j)\Delta V_j \ .\end{aligned} \tag{2.25}$$

Note that a convenient particle weight definition is to use a product rule such as, $\Delta V = \Delta x_1 \Delta x_2$. If $\Delta V_j = 1$, the discrete reproducing equation can be interpreted as a modified Moving Least Square approximation (Liu, Li, and Belytschko, 1996).

In general, $u^{R_h}(\mathbf{x}_j) \neq u(\mathbf{x}_j)$ because $N_i(\mathbf{x}_j) \neq \delta_{ij}$ where δ_{ij} is the Kronecker delta equaling one when $i = j$ and zero otherwise. While the RKPM shape functions cannot be strictly interpreted as an interpolant, for practical purposes it can be viewed as such (Lancaster and Salkauskas, 1981). In order for the nodal coefficients to correspond to the nodal values, the coefficients must be transformed using the RKPM shape functions.

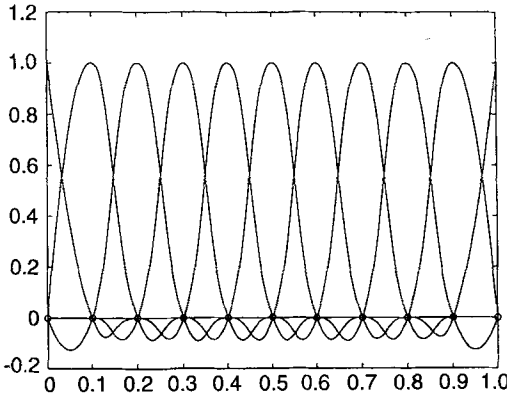

Fig. 1. Kronecker delta condition of quadratic basis shape functions

An interesting property of one dimensional RKPM shape functions, and meshless interpolants in general, occurs when the shape function covers a number of nodes equal to the number of monomials in it basis. For example if a shape function with a quadratic basis (three monomials: $1, x, x^2$) covers three nodes, Kronecker delta shape functions will result as in Fig. 1. Beissel and Belytschko (1996) report that this feature can be extended to higher dimensions with non-concentric weighting functions. In one dimensional boundary value problems, this feature is very advantageous for handling essential boundary conditions.

Derivatives of the shape funcitons are obtained by straight forward differentiation with respect to $\mathbf{x}$. For example the first partial derivatives of linear two dimensional shape functions are

$$\begin{bmatrix} N_{j,x_1}(\mathbf{x}) \\ N_{j,x_2}(\mathbf{x}) \end{bmatrix} = \begin{bmatrix} \{C_{,x_1}(\mathbf{x};\mathbf{x}-\mathbf{x}_j)\phi_{\mathbf{a}_j}(\mathbf{x}-\mathbf{x}_j)+C(\mathbf{x};\mathbf{x}-\mathbf{x}_j)\phi_{\mathbf{a}_j,x_1}(\mathbf{x}-\mathbf{x}_j)\}\Delta V_j \\ \{C_{,x_2}(\mathbf{x};\mathbf{x}-\mathbf{x}_j)\phi_{\mathbf{a}_j}(\mathbf{x}-\mathbf{x}_j)+C(\mathbf{x};\mathbf{x}-\mathbf{x}_j)\phi_{\mathbf{a}_j,x_2}(\mathbf{x}-\mathbf{x}_j)\}\Delta V_j \end{bmatrix} , \tag{2.26}$$

where the derivative of $C(\mathbf{x};\mathbf{x}-\mathbf{x}_j)$ is obtained as follows

$$\begin{aligned}C_{,\mathbf{x}}(\mathbf{x};\mathbf{x}-\mathbf{x}_j) = &\mathbf{P}^T_{,\mathbf{x}}(\mathbf{x}-\mathbf{x}_j)\mathbf{b}(\mathbf{a},\mathbf{x}) \\ &+ \mathbf{P}^T(\mathbf{x}-\mathbf{x}_j)\mathbf{b}_{,\mathbf{x}}(\mathbf{a},\mathbf{x}) \ .\end{aligned} \tag{2.27}$$

3 Incorporation of dilation function

As seen in the previous Section, the standard RKPM formulation allows only for a constant dilation at each node. Thus each node may have an associated window function with an oval or rectangular support in two dimensions; a square and circular support being special cases. In order to form window functions and thus shape functions with arbitrary supports, the reproducing kernel particle method can be extended to naturally include this feature. In the standard definition of the reproducing equation

$$u^{R_a}(\mathbf{x}) = \int_{\Omega_y} u(\mathbf{y})\phi_{\mathbf{a}(\mathbf{y})}(\mathbf{x}-\mathbf{y})\mathrm{d}\Omega_y \ , \tag{3.1}$$

the dilation, $\mathbf{a}(\mathbf{y})$ is viewed only as a function of y in the continuous sense. Thus when the reproducing equation is discretized, the dilation becomes a nodal parameter, a_j.

However, if the continuous reproducing equation is interpreted as follows

$$u^{R_a}(\mathbf{x}) = \int_{\Omega_y} u(\mathbf{y})\phi_{\mathbf{a}(\mathbf{x},\mathbf{y})}(\mathbf{x}-\mathbf{y})\mathrm{d}\Omega_y \ , \tag{3.2}$$

with the dilation defined as $\mathbf{a}(\mathbf{x},\mathbf{y})$, the dilation becomes $\mathbf{a}_j(\mathbf{x})$ when discretized. The end result is a versatile dilation function. With the incorporation of the dilation function, the reproducing conditions of RKPM remain the same as derived in Section 2, and only the window function is modified.

The motivation for a dilation with spatial dependence, is to incorporate the ability to generate conforming shape functions in the context of meshless methods. The term conforming shape function is used here to imply shape functions generated with compactly supported window functions over arbitrary domains. Thus shape functions can be generated over supports other than ovals or rectangles. This property is especially desirable for shape functions near essential boundary conditions.

3.1 Dilation function definitions

The form of the dilation function is similar to that of the standard dilation parameter (Liu, Jun, and Zhang, 1995) and is explicitly defined as the following dot product

$$\mathrm{a}_j(\mathbf{x}) = \mathbf{r}_j(\mathbf{x})\Delta\mathbf{x}_j = \sum_{d=1}^{\eta} N_d^j(\mathbf{x})\mathbf{r}_d\Delta\mathbf{x}_j \ \text{ no sum on } j \ . \tag{3.3}$$

Here, $\mathbf{r}_j(\mathbf{x})$ is a non-dimensional refinement vector associated with a particle and $\Delta\mathbf{x}_j$ is a vector pertaining to the particle weight. Components of the vectors correspond to the space dimensions. The interpolants, $N_d^j(\mathbf{x})$, are used to generate sufficiently smooth dilation functions given a set of η dilation values. Obvious candidates for these interpolants are Lagrange or spline interpolants.

Figure 2 demonstrates the implementation of the above concepts. By using boundary and nodal information, refinement values, $\mathbf{r}_d$, can be selected such that a portion of the shape function's perimeter can represent a boundary modeled by a polynomial curve. The number of points interpolated along the boundary will determine the order of polynomial that can be represented.

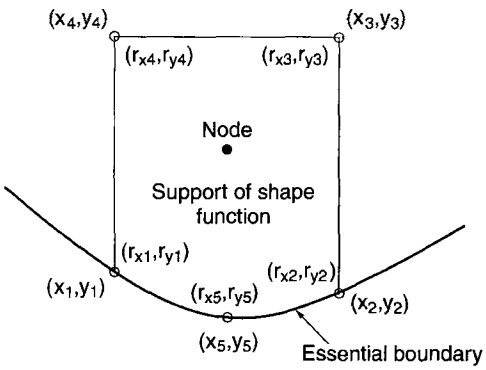

Fig. 2. Conforming shape function diagram near an essential boundary condition

3.2 Window function

The window function, referred to as a weighting function in other meshless methods, is usually a compactly supported function and has the ability to be translated and dilated. It is defined by

$$\phi_{a_j}(\mathbf{x}) = E(a_j)\phi\left(\frac{\mathbf{x}-\mathbf{x}_j}{a_j(\mathbf{x})}\right) \ , \tag{3.4}$$

where $E(a_j)$ is a normalization factor that ensures the area of the window is equal to one.

While the choice of the optimal window remains an open issue, the cubic spline has been a popular choice due to its compact support, explicit form, and smoothness. The one dimensional cubic spline window is defined as

$$\phi_{a_j(x)} = E(a_j)\begin{cases} \frac{1}{6}(z+2)^3 & \text{for } -2 \le z < -1 \\ \frac{2}{3} - z^2(1+\frac{z}{2}) & \text{for } -1 \le z < 0 \\ \frac{2}{3} - z^2(1-\frac{z}{2}) & \text{for } 0 \le z < 1 \\ -\frac{1}{6}(z-2)^3 & \text{for } 1 \le z \le 2 \\ 0 & \text{for } |z| > 2 \end{cases} \tag{3.5}$$

where the following transformation is used

$$z = \frac{x - x_j}{a_j(x)} \ .$$

With the addition of the dilation function, the derivative of the cubic spline window is

$$\phi'_{a_j(x)=E(a_j)}\begin{cases} \frac{1}{2}(z+2)^2\mathrm{d}z & \text{for } -2 \le z < -1 \\ -z(\frac{3}{2}z+2)\mathrm{d}z & \text{for } -1 \le z < 0 \\ z(\frac{3}{2}z-2)dz & \text{for } 0 \le z < 1 \\ -\frac{1}{2}(z-2)^2\mathrm{d}z & \text{for } 1 \le z \le 2 \\ 0 & \text{for } |z| > 2 \end{cases} \tag{3.6}$$

where

$$\mathrm{d}z = \frac{1}{a_j(x)} - a_j'(x)\frac{x-x_j}{a_j^2(x)} \ ,$$

and $a_j'(x)$ is obtained from differentiating Eq. (3.3) and multiplying by the particle weight. Figure 3 shows a symmetric window generated with a constant dilation and a skewed window obtained with a linear dilation function.

It is reiterated that the normalization factor $E(a_j)$ is a constant used to normalize the window. With the dilation function, the normalization factor in the continuous sense is defined as

$$E(a_j) = \int\left\{\frac{1}{a_j(x)} - a_j'(x)\frac{x-x_j}{a_j^2(x)}\right\}\mathrm{d}x \ . \tag{3.7}$$

While the introduction of spatial dependence on the dilation complicates the normalization, it is not necessary to

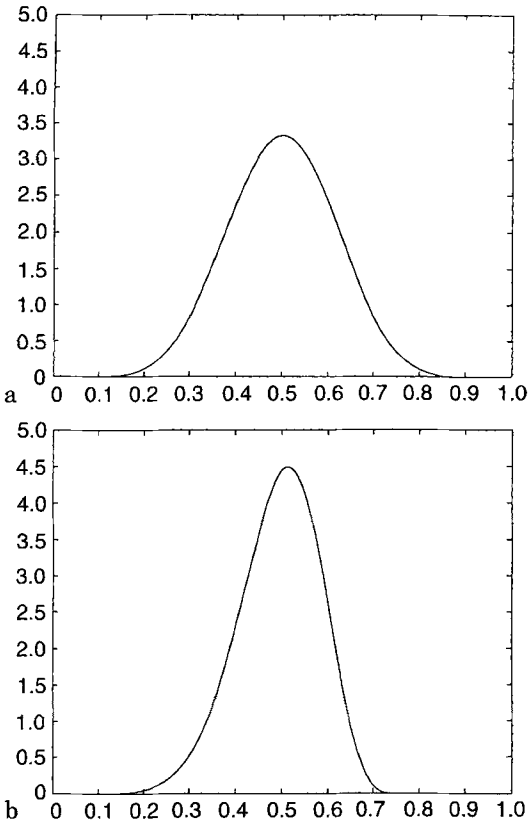

Fig. 3. a,b. Symmetric window with constant dilation and skewed window with linear dilation function. **(a)** Symmetric window. **(b)** Skewed window

differentiate it when taking the derivative of the window function since its only purpose is to normalize the window. Moreover, the normalization factor is not a strict requirement and in the discrete case could be approximated or even neglected as in other meshless methods.

4
The (Bubnov-) Galerkin method

4.1
Overview

While variations of the Galerkin method have been widely applied to meshless methods, a strict application of the (Bubnov-) Galerkin method has not. Following the approach of Hughes (1987), the (Bubnov-) Galerkin method, commonly referred to as simply the Galerkin method, uses two sets of functions to formulate a variational form of the strong form. One set consists of trial functions and the other consists of test functions.

$$\mathcal{S} = \{u | u \in H^1, u = g \text{ on } \Gamma_g\} \text{ (trial functions)} \quad (4.1a)$$

$$\mathcal{V} = \{w | w \in H^1, w = 0 \text{ on } \Gamma_g\} \text{ (test functions)} \quad (4.1b)$$

The boundary of the domain is defined by the following

$$\Gamma_g \cup \Gamma_h = \Gamma \quad \text{(boundary)} \quad (4.2a)$$

$$\Gamma_g \cap \Gamma_h = \emptyset \quad \text{(empty set)} \ , \quad (4.2b)$$

where Γ_g is an essential boundary, Γ_h is a natural boundary and g is the prescribed essential boundary condition.

The discretized test functions in meshless methods typically do not satisfy the condition that they vanish on the essential boundary. However, by selectively choosing the dilation, window and particle distribution, RKPM shape functions can be devised such that the following finite dimensional approximations of $\mathcal{S}$ and $\mathcal{V}$, denoted $\mathcal{S}^h$ and $\mathcal{V}^h$ respectively, satisfy the following

$$\mathcal{S}^h = \{u^h | u^h \in H^1, u^h = g^h \text{ on } \Gamma_g\} \quad (4.3a)$$

$$\mathcal{V}^h = \{w^h | w^h \in H^1, w^h = 0 \text{ on } \Gamma_g\} \ , \quad (4.3b)$$

where $\mathcal{S}^h$ and $\mathcal{V}^h$ are subsets of $\mathcal{S}$ and $\mathcal{V}$. While it is required that u^h and $w^h \in H^1$ for 2nd order problems, RKPM shape functions can be H^m, or continuous to any degree for higher order problems.

In the classical Galerkin approach, the trial functions are defined to consist of the following approximations

$$u^h = v^h + g^h \ , \quad (4.4)$$

where v^h are usually taken identical to w^h, the test function approximations, and g^h are arbitrary approximations used to represent the prescribed essential boundary condition. It is important to note that unlike current meshless method test functions, all members of v^h vanish on Γ_g in this formulation.

The approximations of v^h, g^h, and w^h consist of the following interpolation expressions

$$v^h(\mathbf{x}) = \sum_{j \in NP - \eta_g} N_j(\mathbf{x}) v(\mathbf{x}_j) \quad (4.5)$$

$$g^h(\mathbf{x}) = \sum_{j \in \eta_g} \tilde{N}_j(\mathbf{x}) g(\mathbf{x}_j) \quad (4.6)$$

$$w^h(\mathbf{x}) = \sum_{j \in NP - \eta_g} N_j(\mathbf{x}) w(\mathbf{x}_j) \ , \quad (4.7)$$

where $N_j(\mathbf{x})$ are standard RKPM shape functions and $\tilde{N}_j(\mathbf{x})$ are constructed from reproducing conditions such that completeness is maintained throughout the domain (Liu, Chen, and Uras, 1995). The variable η_g denotes the set of nodes that reside on the essential boundary.

To clarify the above formulation, the discretization of a one dimensional domain with *NP* nodes is presented in Fig. 4. For illustrative purposes, the boundary points are comprised of an essential boundary condition Γ_g on the left and a natural boundary condition Γ_g on the right. The nodes not associated with the essential boundary are numbered from 1 thru *neq* where *neq* represents the number of global equations to be solved. The node belonging to the essential boundary is labeled *neq*+1. Thus, $neq + 1 \in \eta_g$ and $1, ..., neq \in NP - \eta_g$. The approximations, v^h and w^h, can then be comprised of identical shape functions associated with the particles belonging to the set, $NP - \eta_g$, while the essential boundary condition on Γ_g is represented with $N_{neq+1}(\Gamma_g)$. The trial and test collections are comprised of the following shape functions,

$$\mathcal{S}^h = \{N_1, N_2, ..., N_{neq}, N_{neq+1}\} \quad (4.8)$$

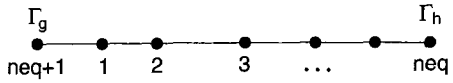

Fig. 4. Nodal numbering for one dimensional Galerkin description

$$\mathcal{V}^h = \{N_1, N_2, ..., N_{neq}\} \ . \tag{4.9}$$

Unlike the finite element method in which the shape satisfy the Kronecker delta condition, RKPM shape functions in general do not. Therefore nodal displacements must be imposed indirectly on the global system of equations. For example, to represent $g^h(x)$ on Γ_g over the nodes belonging to η_g with the approximation of Eq. (4.6), the nodal displacements, $g(\mathbf{x}_A)$, are obtained by solving a linear system of equations. For $\{1, ..., n\} \in \eta_g$ the following system would result.

$$\begin{bmatrix} N_1(\mathbf{x}_1) & N_2(\mathbf{x}_1) & \dots & N_n(\mathbf{x}_1) \\ N_1(\mathbf{x}_2) & N_2(\mathbf{x}_2) & \dots & N_n(\mathbf{x}_2) \\ \vdots & \vdots & \ddots & \vdots \\ N_1(\mathbf{x}_n) & N_2(\mathbf{x}_n) & \dots & N_n(\mathbf{x}_n) \end{bmatrix} \begin{bmatrix} g(\mathbf{x}_1) \\ g(\mathbf{x}_2) \\ \vdots \\ g(\mathbf{x}_n) \end{bmatrix}$$

$$= \begin{bmatrix} g^h(\mathbf{x}_1) \\ g^h(\mathbf{x}_2) \\ \vdots \\ g^h(\mathbf{x}_n) \end{bmatrix} \ . \tag{4.10}$$

Having evaluated the nodal values on the essential boundary, the global matrix equation can be manipulated in the usual FEM manner to enforce the essential boundary condition. The global system is thereby reduced to the number of degrees of freedom for the particles belonging to $NP - \eta_g$. The stiffness matrix also remains positive definite, banded, and symmetric for the case when v^h is identical to w^h.

4.2 Elastostatic formulation

Linear elastostatics can be posed in the following manner,

$$\nabla \cdot \boldsymbol{\sigma} + \mathbf{f} = 0 \quad \text{in} \quad \Omega \tag{4.11a}$$

$$\mathbf{u} = \mathbf{g} \qquad \text{on} \quad \Gamma_g \tag{4.11b}$$

$$\mathbf{n} \cdot \boldsymbol{\sigma} = \mathbf{h} \qquad \text{on} \quad \Gamma_h \ , \tag{4.11c}$$

where $\boldsymbol{\sigma}$ is the Cauchy stress tensor, $\mathbf{f}$ is a body force, $\mathbf{g}$ is the prescribed displacement on the essential boundary Γ_g and $\mathbf{h}$ is the prescribed traction on the natural boundary Γ_h.

The constitutive relation is

$$\sigma_{ij} = C_{ijkl}\epsilon_{kl} \ , \tag{4.12}$$

where the strain-displacement equation is

$$\epsilon_{kl} = \frac{1}{2}(u_{k,l} + u_{l,k}) \ . \tag{4.13}$$

The strong form is multiplied by the test function and integrated over the domain to obtain the weak form

$$a(\mathbf{w}, \mathbf{u}) = (\mathbf{w}, \mathbf{f}) + (\mathbf{w}, \mathbf{h})_\Gamma \ . \tag{4.14}$$

where $a(\cdot, \cdot)$ and $(\cdot, \cdot)$ are symmetric bilinear operators defined by

$$a(\mathbf{w}, \mathbf{u}) = \int_\Omega w_{(i,j)} c_{ijkl} v_{(k,l)} \mathrm{d}\Omega \ , \tag{4.15a}$$

$$(\mathbf{w}, \mathbf{f}) = \int_\Omega w_i f_i \mathrm{d}\Omega \ , \tag{4.15b}$$

$$(\mathbf{w}, \mathbf{h})_\Gamma = \sum_{i=1}^{nsd} \left(\int_{\Gamma_{h_i}} w_i h_i \mathrm{d}\Gamma \right) \ . \tag{4.15c}$$

Substituting the shape function approximations, the matrix form is obtained from the following Galerkin form

$$a(\mathbf{w}^\mathbf{h}, \mathbf{v}^\mathbf{h}) = (\mathbf{w}^\mathbf{h}, \mathbf{f}) + (\mathbf{w}^\mathbf{h}, \mathbf{h})_\Gamma - a(\mathbf{w}^\mathbf{h}, \mathbf{g}^\mathbf{h}) \ . \tag{4.16}$$

5 Implementation of admissible approximations

This Section provides conditions for generating admissible shape functions in the proximity of essential boundaries by forcing either the correction function or window function equal to zero at the boundary. For one dimensional problems both methods are fairly straightforward and shed light on the main concepts of constructing admissible approximations. In two dimensions matters are more complicated in that boundaries can take on many different shapes. Curved as well as straight boundaries will be addressed.

5.1 Forcing the correction function to equal zero

5.1.1 One dimension

In the one dimensional case, for all v^h to vanish at the boundary, the Kronecker delta condition must exist at that boundary. Consequently, the essential boundary condition can be enforced simply by setting the nodal coefficient equal to the prescribed value in the global matrix equation, avoiding the procedure of transforming the nodal coefficients as described in Section 4.

In order for the shape functions near the essential boundary condition to satisfy the above conditions through the correction function, the associated dilations must be chosen in accordance to the Kronecker delta conditions of Section 2. Consequently for a linear basis, the shape function at the boundary must cover two nodes and likewise, for a quadratic basis, the shape function must cover three nodes.

To verify the Kronecker delta condition at the essential boundary condition for a linear basis, it can be shown using the notation of Fig. 5 that

$$N_1(x) = C(x; x - x_1)\phi_{a_1}(x - x_1)\Delta x_1 = 1 \quad \text{at } x = x_1 \ , \tag{5.1}$$

where $C(x; x - x_1) = b_0(a, x) + b_1(a, x)(x - x_1)$. Evaluating the shape function at $x = x_1$ simplifies Eq. (5.1) yielding

Fig. 5. One dimensional particle distribution notation near an essential boundary condition

$$N_1(x_1) = b_0(a,x_1)\phi_{a_1}(0)\Delta x_1 \ . \tag{5.2}$$

The correction coefficients, $b_0(a,x_1)$ and $b_1(a,x_1)$, are obtained from one dimensional linear reproducing conditions as described in Section 2.

$$\begin{bmatrix} \tilde{m}_0(a,x) & \tilde{m}_1(a,x) \\ \tilde{m}_1(a,x) & \tilde{m}_2(a,x) \end{bmatrix} \begin{bmatrix} b_0(a,x_1) \\ b_1(a,x_1) \end{bmatrix} = \begin{bmatrix} 1 \\ 0 \end{bmatrix} , \tag{5.3}$$

where $\tilde{m}_0(a,x)$, $\tilde{m}_1(a,x)$ and $\tilde{m}_2(a,x)$ are the discrete moments of the moment matrix.

Representing $b_0(a,x_1)$ in terms of discrete moments and substituting into Eq. (5.2) yields

$$N_1(x_1) = \frac{\tilde{m}_2(a,x_1)}{\tilde{m}_0(a,x_1)\tilde{m}_2(a,x_1) - \tilde{m}_1(a,x_1)^2}\phi_{a_1}(0)\Delta x_1 \ . \tag{5.4}$$

Evaluating the moments for the case in which the dilation parameters are selected such that only two nodes contribute at the boundary yields

$$\begin{aligned} \tilde{m}_0 &= \sum_{j=1}^{np} \phi_{a_j}(x - x_j)\Delta x_j = \phi_{a_1}(0)\Delta x_1 \\ &\quad + \phi_{a_2}\left(\frac{x_1 - x_2}{a_2}\right)\Delta x_2 \\ \tilde{m}_1 &= \sum_{j=1}^{np}(x - x_j)\phi_{a_j}(x - x_j)\Delta x_j \\ &= (x_1 - x_2)\phi_{a_2}\left(\frac{x_1 - x_2}{a_2}\right)\Delta x_2 \\ \tilde{m}_2 &= \sum_{j=1}^{np}(x - x_j)^2\phi_{a_j}(x - x_j)\Delta x_j \\ &= (x_1 - x_2)^2\phi_{a_2}\left(\frac{x_1 - x_2}{a_2}\right)\Delta x_2 \ . \end{aligned} \tag{5.5}$$

By representing $\tilde{m}_2$ is terms of $\tilde{m}_1$

$$\tilde{m}_2 = (x_1 - x_2)\tilde{m}_1 \ , \tag{5.6}$$

a factor of $\tilde{m}_1$ can be canceled out of Eq. (5.4) giving,

$$N_1(x_1) = \frac{(x_1 - x_2)}{(x_1 - x_2)\tilde{m}_0 - \tilde{m}_1}\phi_{a_1}(0)\Delta x_1 \ . \tag{5.7}$$

Noting from Eq. (5.5) that

$$(x_1 - x_2)\tilde{m}_0 = (x_1 - x_2)\phi_{a_1}(0)\Delta x_1 + \tilde{m}_1 \ , \tag{5.8}$$

a final form is obtained that is clearly equal to 1.

$$N_1(x_1) = \frac{(x_1 - x_2)\phi_{a_1}(0)\Delta x_1}{(x_1 - x_2)\phi_{a_1}(0)\Delta x_1} = 1 \ . \tag{5.9}$$

By showing that the shape function associated with the node at the boundary is equal to 1, it can be concluded that all interior shape functions must vanish at the boundary to satisfy consistency.

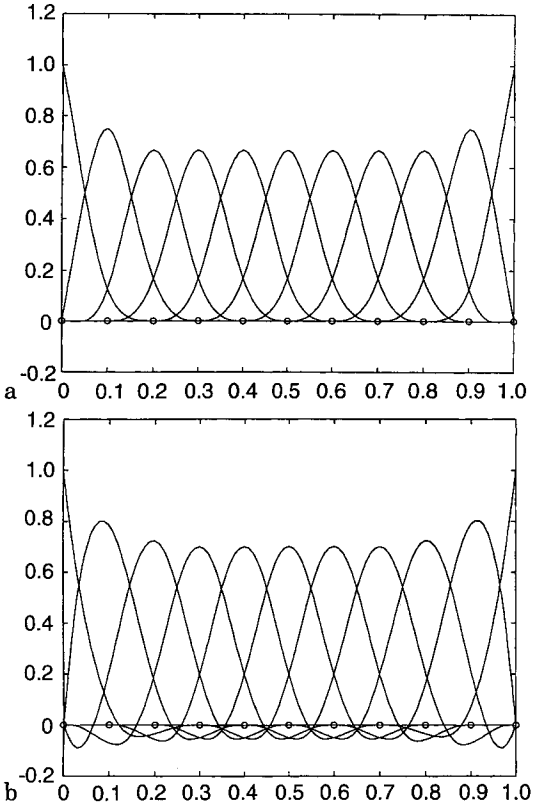

Fig. 6. a,b. Kronecker delta property of shape functions at boundary achieved by choosing dilations such that the correction function of the node adjacent to the boundary equals zero at the boundary. (**a**) Linear basis. (**b**) Quadratic basis

The above condition holds for any compactly supported window function. The dilation criteria near the essential boundary to generate admissible linear and quadratic basis shape functions for the Galerkin method is given by the following equations.

$$\text{linear basis} : \begin{cases} \frac{x_2 - x_1}{z_{bnd}} < & a_1 < \frac{x_3 - x_1}{z_{bnd}} \\ \frac{x_2 - x_1}{z_{bnd}} < & a_2 < \frac{x_3 - x_1}{z_{bnd}} \\ & a_n < \frac{x_n - x_1}{z_{bnd}} \end{cases} \quad n = 3, \cdots, NP$$

$$\text{quadratic basis} : \begin{cases} \frac{x_3 - x_1}{z_{bnd}} < & a_1 < \frac{x_4 - x_1}{z_{bnd}} \\ \frac{x_3 - x_1}{z_{bnd}} < & a_2 < \frac{x_4 - x_1}{z_{bnd}} \\ & a_n < \frac{x_n - x_1}{z_{bnd}} \end{cases} \quad n = 3, \cdots, NP$$

where it is assumed the window function has been defined to be nonzero over the range $[-z_{bnd}, z_{bnd}]$. For example, $z_{bnd} = 2$ for the cubic spline window function given in Section 3. The above equations are valid for nonuniform as well as uniform particle distributions. Examples of one dimensional admissible shape functions for linear and quadratic bases are depicted in Fig. 6.

5.1.2 Two dimensions

In two dimensions, the requirement of the shape functions in the proximity of an essential boundary equal to zero at the boundary as a result of the correction function equaling zero is much more involved than in the one dimensional case. An example for which this occurs follows

for a uniform discretization, of grid size h_x by h_y, along the boundary as depicted in Fig. 7. Constant dilations of $a_x = h_x$ and $a_y = h_y$ along with a linear basis are assumed. By evaluating the correction function at an arbitrary point along the boundary $(\bar{x}, -h_y)$ for a particle J located at (0,0), it will be shown that with the proper choice of window function, shape functions adjacent to an essential boundary can vanish at every point along the boundary making them admissible.

From the definition of the RKPM shape function

$$N_J(\mathbf{x}) = C(\mathbf{x}; \mathbf{x} - \mathbf{x}_J)\phi_{\mathbf{a}_J}(\mathbf{x} - \mathbf{x}_J)\Delta V_J \ , \tag{5.10}$$

we see that if the correction function $C(\mathbf{x}; \mathbf{x} - \mathbf{x}_J)$ equals zero, then the shape function will also equal zero. The correction function for a linear basis is defined as

$$C(\mathbf{x}; \mathbf{x} - \mathbf{x}_J) = b_{00}(\mathbf{a}, \mathbf{x}) + b_{10}(\mathbf{a}, \mathbf{x})(x - x_J) + b_{01}(\mathbf{a}, \mathbf{x})(y - y_J) \ . \tag{5.11}$$

In solving for the correction coefficients, the discrete moment matrix is inverted and multiplied by $\mathbf{P}(\mathbf{0})$ yielding

$$\mathbf{b}(\mathbf{a}, \mathbf{x}) = \tilde{\mathbf{M}}(\mathbf{a}, \mathbf{x})^{-1}\mathbf{P}(\mathbf{0}) \ . \tag{5.12}$$

By setting $C(\mathbf{x}; \mathbf{x} - \mathbf{x}_J)$ equals to zero and factoring out the determinant of the moment matrix, the following is obtained.

$$A_{11} - A_{12}(x - x_J) + A_{13}(y - y_J) = 0 \ , \tag{5.13}$$

where A_{11}, and A_{12}, and A_{13} are the cofactors of $\tilde{\mathbf{M}}(a, x)$ defined by

$$A_{11} = \tilde{m}_{20}\tilde{m}_{02} - \tilde{m}_{11}^2 \tag{5.14a}$$

$$A_{12} = \tilde{m}_{10}\tilde{m}_{02} - \tilde{m}_{11}\tilde{m}_{01} \tag{5.14b}$$

$$A_{13} = \tilde{m}_{10}\tilde{m}_{11} - \tilde{m}_{20}\tilde{m}_{01} \ . \tag{5.14c}$$

Evaluating the discrete moments at $(\bar{x}, -h_y)$ yields the following

$$\begin{aligned}\tilde{m}_{10} &= \sum_{j=1}^{np}(x - x_j)\phi_{a_j}(\mathbf{x} - \mathbf{x}_j)\Delta V_j \\ &= \left\{x_1\phi_x\left(\frac{x_1}{h_x}\right) + x_2\phi_x\left(\frac{x_2}{h_x}\right) + x_3\phi_x\left(\frac{x_3}{h_x}\right) + x_4\phi_x\left(\frac{x_4}{h_x}\right)\right\}\phi_y(0)\frac{h_xh_y}{2} \\ &\quad + \left\{x_1\phi_x\left(\frac{x_1}{h_x}\right) + x_2\phi_x\left(\frac{x_2}{h_x}\right) + x_3\phi_x\left(\frac{x_3}{h_x}\right) + x_4\phi_x\left(\frac{x_4}{h_x}\right)\right\}\phi_y(1)h_xh_y\end{aligned}$$

$$\begin{aligned}\tilde{m}_{01} &= \sum_{j=1}^{np}(y - y_j)\phi_{a_j}(\mathbf{x} - \mathbf{x}_j)\Delta V_j \\ &= -h_y\left\{\phi_x\left(\frac{x_1}{h_x}\right) + \phi_x\left(\frac{x_2}{h_x}\right) + \phi_x\left(\frac{x_3}{h_x}\right) + \phi_x\left(\frac{x_4}{h_x}\right)\right\}\phi_y(1)h_xh_y\end{aligned}$$

$$\begin{aligned}\tilde{m}_{11} &= \sum_{j=1}^{np}(x - x_j)(y - y_j)\phi_{a_j}(\mathbf{x} - \mathbf{x}_j)\Delta V_j \\ &= -h_y\left\{x_1\phi_x\left(\frac{x_1}{h_x}\right) + x_2\phi_x\left(\frac{x_2}{h_x}\right) + x_3\phi_x\left(\frac{x_3}{h_x}\right) + x_4\phi_x\left(\frac{x_4}{h_x}\right)\right\}\phi_y(1)h_xh_y \qquad (5.15)\end{aligned}$$

$$\begin{aligned}\tilde{m}_{20} &= \sum_{j=1}^{np}(x - x_j)^2\phi_{a_j}(\mathbf{x} - \mathbf{x}_j)\Delta V_j \\ &= \left\{x_1^2\phi_x\left(\frac{x_1}{h_x}\right) + x_2^2\phi_x\left(\frac{x_2}{h_x}\right) + x_3^2\phi_x\left(\frac{x_3}{h_x}\right) + x_4^2\phi_x\left(\frac{x_4}{h_x}\right)\right\}\phi_y(0)\frac{h_xh_y}{2} \\ &\quad + \left\{x_1^2\phi_x\left(\frac{x_1}{h_x}\right) + x_2^2\phi_x\left(\frac{x_2}{h_x}\right) + x_3^2\phi_x\left(\frac{x_3}{h_x}\right) + x_4^2\phi_x\left(\frac{x_4}{h_x}\right)\right\}\phi_y(1)h_xh_y\end{aligned}$$

$$\begin{aligned}\tilde{m}_{02} &= \sum_{j=1}^{np}(y - y_j)^2\phi_{a_j}(\mathbf{x} - \mathbf{x}_j)\Delta V_j \\ &= -h_y^2\left\{\phi_x\left(\frac{x_1}{h_x}\right) + \phi_x\left(\frac{x_2}{h_x}\right) + \phi_x\left(\frac{x_3}{h_x}\right) + \phi_x\left(\frac{x_4}{h_x}\right)\right\}\phi_y(1)h_xh_y\end{aligned}$$

where np, the number of particles that contribute to the moment calculations, equals 8 for the example depicted in Fig. 7 and

$$\begin{aligned}x_1 &= x_5 = \bar{x} + h_x \\ x_2 &= x_6 = \bar{x} \\ x_3 &= x_7 = \bar{x} - h_x \\ x_4 &= x_8 = \bar{x} - 2h_x \ .\end{aligned}$$

Substituting the cofactor expressions into Eq. (5.13) and evaluating at particle J located at (0,0) as in Fig. 7, gives

$$(\tilde{m}_{20}\tilde{m}_{02} - \tilde{m}_{11}^2) - (\tilde{m}_{10}\tilde{m}_{02} - \tilde{m}_{11}\tilde{m}_{01})(\bar{x}) + (\tilde{m}_{10}\tilde{m}_{11} - \tilde{m}_{20}\tilde{m}_{01})(h_y) = 0 \ . \tag{5.16}$$

From the moment calculations, the following relations from Eq. 5.15 can be used to simplify Eq. (5.16).

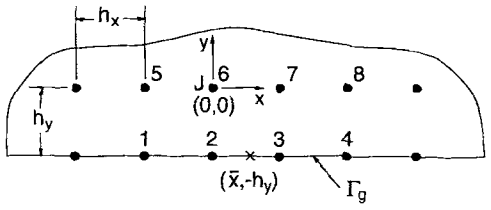

Fig. 7. Particle distribution along a straight essential boundary that enables the correction function to vanish at boundary

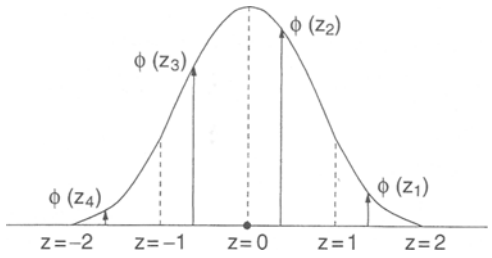

Fig. 8. Window moment symmetry condition of cubic spline window, $m_w = z_1\phi(z_1) + z_2\phi(z_2) + z_3\phi(z_3) + z_4\phi(z_4) = 0$, where $z_1 = z_2 + 1 = z_3 + 2 = z_4 + 3$

$$\tilde{m}_{01} = -h_y \tilde{m}_{02} \tag{5.17}$$

$$\tilde{m}_{10} = \phi_y(0)\frac{h_x h_y}{2}\left\{x_1\phi_x\left(\frac{x_1}{h_x}\right) + x_2\phi_x\left(\frac{x_2}{h_x}\right) + x_3\phi_x\left(\frac{x_3}{h_x}\right) + x_4\phi_x\left(\frac{x_4}{h_x}\right)\right\} - \tilde{m}_{11} \ . \tag{5.18}$$

For ease of presentation, the following definition is used

$$\begin{aligned} m_w &= x_1\phi_x\left(\frac{x_1}{h_x}\right) + x_2\phi_x\left(\frac{x_2}{h_x}\right) \\ &\quad + x_3\phi_x\left(\frac{x_3}{h_x}\right) + x_4\phi_x\left(\frac{x_4}{h_x}\right) \ , \\ &= (\bar{x} + h_x)\phi_x\left(\frac{\bar{x} + h_x}{h_x}\right) + \bar{x}\phi_x\left(\frac{\bar{x}}{h_x}\right) \\ &\quad + (\bar{x} - h_x)\phi_x\left(\frac{\bar{x} - h_x}{h_x}\right) \\ &\quad + (\bar{x} - 2h_x)\phi_x\left(\frac{\bar{x} - 2h_x}{h_x}\right) \ . \end{aligned} \tag{5.19}$$

Equation (5.16) can now be expressed as

$$-(\tilde{m}_{10}\tilde{m}_{02} - \tilde{m}_{11}\tilde{m}_{01})\bar{x} + m_w\tilde{m}_{11} = 0 \ . \tag{5.20}$$

Further simplification using Eq. (5.18) yields

$$-m_w\tilde{m}_{02}\bar{x} + m_w\tilde{m}_{11} = 0 \ , \tag{5.21a}$$

$$m_w(\tilde{m}_{11} - \tilde{m}_{02}\bar{x}) = 0 \ . \tag{5.21b}$$

The most obvious way for Eq. (5.21b) to equal zero is for m_w to equal zero. This expression is only dependent upon the type of window function and particle distribution. By direct substitution, it can be verified that the cubic spline window given in Section 2 satisfies this condition which can be thought of as a *moment symmetry condition* of the window function (see Fig. 8). A shape function for particle J is plotted in Fig. 9. Note that while the above proof was given for a boundary coincident with the coordinate axes, orthogonality is not necessary for this condition to hold.

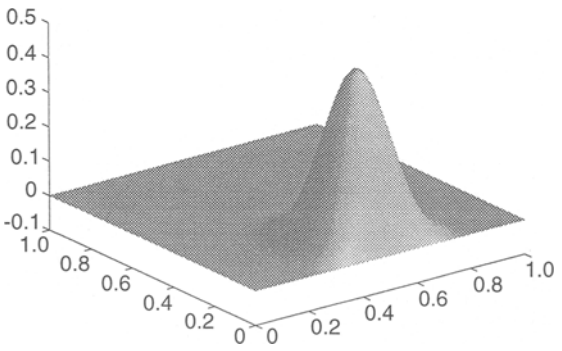

Fig. 9. Linear basis shape function near straight boundary in which correction function equals zero along the entire boundary

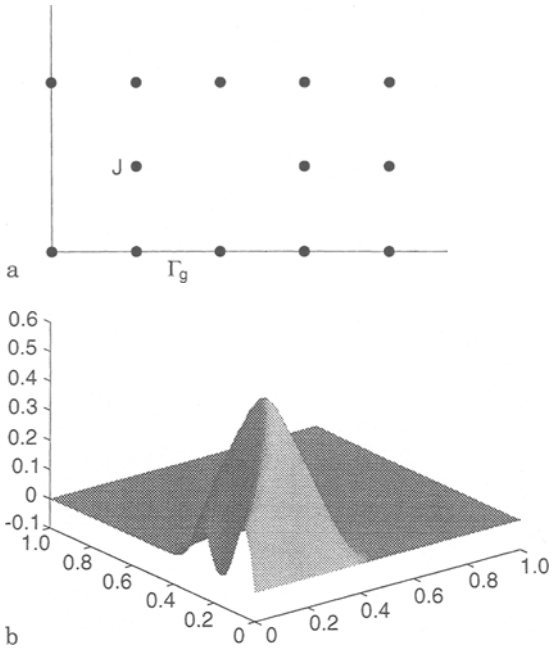

Fig. 10. a,b. Linear basis shape function (corresponding to particle J) near the edge of an essential boundary condition. (**a**) Particle distribution near edge of essential boundary. (**b**) Particle J shape function

In the presence of an edge or other deviation from the straight boundary, the above conditions do not hold. Measures can be taken however to avoid these difficulties. An example is an essential boundary condition prescribed along one side of a rectangular geometry. By using the particle distribution in Fig. 10(a), shape functions can be generated near the boundary that will vanish at the essential boundary provided the proper choice of window, dilation, and particle weights are used. An admissible shape function near the edge of the essential boundary is shown in Fig. 10(b).

5.2
Forcing the window function to equal zero

5.2.1
One dimension

As mentioned earlier, admissible shape functions may also be generated by forcing the window function to vanish at essential boundaries. However, in the one dimensional case this results in an undefined shape function (belonging to η_g) at the boundary point. Assuming that the only contributing node at the boundary is the boundary node itself, evaluating the moments from Eq. (5.5) yields

$$\tilde{m}_0 = \phi_{a_1}(0)\Delta x_1$$
$$\tilde{m}_1 = 0 \qquad (5.22)$$
$$\tilde{m}_2 = 0 \ .$$

From the shape function definition of Eq. (5.2) the following results

$$N_1(x_1) = \frac{0}{0}\phi_{a_1}(0)\Delta x_1 \ . \qquad (5.23)$$

In the limit, however, $N_1(x_1)$ can be taken equal to 1. This can be seen by evaluating N_1 in the limit at a point near the boundary, $x_1 + \varepsilon$ as ε goes to zero. While an arbitrary number of nodes can contribute $x_1 + \varepsilon$, for illustrative purposes, only two nodes will considered. Thus the 1D discrete moments, evaluated at ε (taking $x_1 = 0$), are

$$\tilde{m}_0(\varepsilon) = \phi_{a_1}(\varepsilon)\Delta x_1 + \phi_{a_2}(\varepsilon - x_2)\Delta x_2$$
$$\tilde{m}_1(\varepsilon) = \varepsilon\phi_{a_1}(\varepsilon)\Delta x_1 + (\varepsilon - x_2)\phi_{a_2}(\varepsilon - x_2)\Delta x_2$$
$$\tilde{m}_2(\varepsilon) = \varepsilon^2\phi_{a_1}(\varepsilon)\Delta x_1 + (\varepsilon - x_2)^2\phi_{a_2}(\varepsilon - x_2)\Delta x_2 \ . \qquad (5.24)$$

Evaluating $N_1(\varepsilon)$ yields

$$N_1(\varepsilon) = C(\varepsilon; \varepsilon - x_1)\phi_{a_1}(\varepsilon)\Delta x_1$$
$$= \left\{ \frac{\tilde{m}_2}{\tilde{m}_0\tilde{m}_2 - \tilde{m}_1^2} - \frac{\tilde{m}_1}{\tilde{m}_0\tilde{m}_2 - \tilde{m}_1^2}(\varepsilon) \right\} \phi_{a_1}(\varepsilon)\Delta x_1 \ . \qquad (5.25)$$

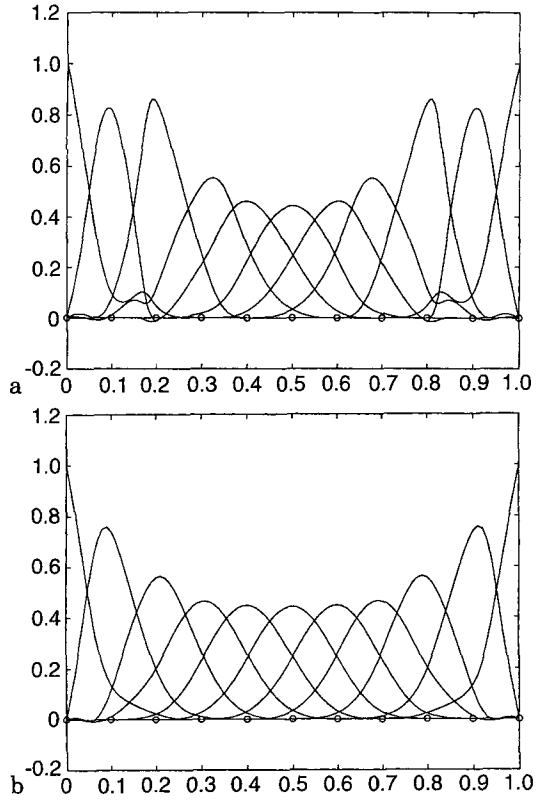

Fig. 11. a,b. Linear shape functions with window forced to zero at boundary. **(a)** Constant dilation. **(b)** Linear dilation function

Dropping the second term of the correction function that is multiplied by ε and substituting the expressions for the moments, gives the following after simplification

$$N_1(\varepsilon) = \left\{ \frac{\varepsilon^2\phi_{a_1}(\varepsilon)\Delta x_1 + (\varepsilon - x_2)^2\phi_{a_2}(\varepsilon - x_2)\Delta x_2}{x_2^2\phi_{a_1}(\varepsilon)\phi_{a_2}(\varepsilon - x_2)\Delta x_1\Delta x_2} \right\} \times \phi_{a_1}(\varepsilon)\Delta x_1 \qquad (5.26)$$
$$= \left\{ \frac{\varepsilon^2}{x_2^2\phi_{a_2}(\varepsilon - x_2)\Delta x_2} + \frac{(\varepsilon - x_2)^2}{x_2^2\phi_{a_1}(\varepsilon)\Delta x_1} \right\} \times \phi_{a_1}(\varepsilon)\Delta x_1 \ .$$

Finally, taking the limit of Eq. 5.26 gives the desired result

$$N_1(x_1) = \lim_{\varepsilon \to 0} N_1(x_1 + \varepsilon)$$
$$= \frac{x_2^2}{x_2^2\phi_{a_1}(\varepsilon)\Delta x_1} \times \phi_{a_1}(\varepsilon)\Delta x_1 = 1, \text{ where } x_1 = 0 \ . \qquad (5.27)$$

Figure 11 shows two methods of forcing the window function to equal zero at the boundary. The first (Fig. 11(a)) uses a constant dilation for each node defined by the distance the particle is from the essential boundary. For instance, the particle nearest the boundary has a dilation that covers three nodes and likewise, the adjacent particle has a dilation that covers five nodes. The irregular shape functions produced by this procedure can be alleviated by incorporating a linear dilation functions in the shape function near the boundary. The linear dilation function used in Fig. 11(b) enables the shape functions near the boundary to die down quickly near the boundary while extend further into the domain opposite the boundary.

5.2.2 Two dimensions

To avoid the restrictions of the particle distribution, dilation, and window function near a straight essential boundary in two dimensions, the dilation can be selected such that the window function will equal zero at the boundary as in the one dimensional case above.

In doing this however, shape functions associated with the essential boundary cannot be evaluated along the boundary with the standard two dimensional RKPM shape function calculation. As will be shown, the 2D calculation degenerates into a 1D calculation along the boundary. Thus for boundary shape functions along a straight essential boundary, a 2D shape function calculation can be used in the interior of the domain and a 1D calcuation can be superimposed along the boundary.

Degeneration in two dimensions occurs when a group of particles fails to define a plane, or in other words, the particles fall on a straight line. Thus even though a given particle distribution may be sufficient, the dilations of distribution may be such that the moment matrix becomes singular. Referring back to Fig. 7, at the boundary $(y - y_j)$ equals zero for approximations at the boundary. Moments

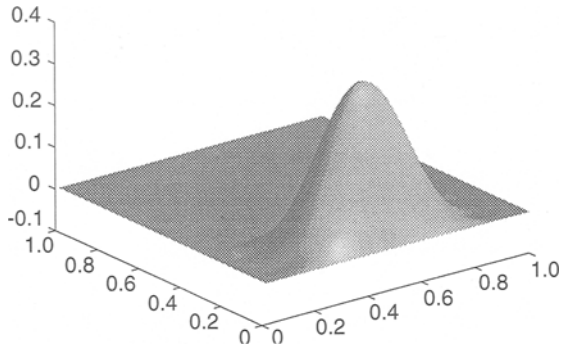

Fig. 12. Linear basis shape function near straight boundary in which window function is forced to zero at boundary

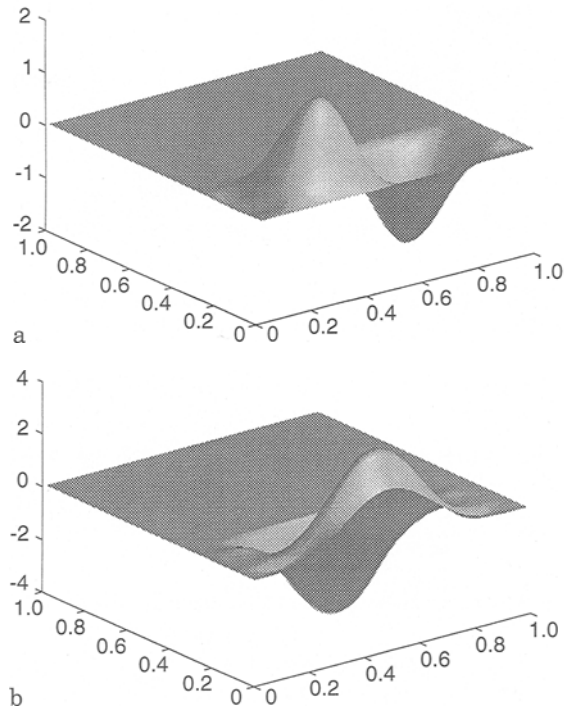

Fig. 13. a,b. Derivatives of linear shape basis function near boundary. (a) Derivative with respect to x. (b) Derivative with respect to y

associated with the y-direction therefore provide no contribution

$$\tilde{m}_{01} = \sum_{j=1}^{np} (y - y_j)\phi_{a_j}(\mathbf{x} - \mathbf{x}_j)\Delta V_j = 0$$

$$\tilde{m}_{11} = \sum_{j=1}^{np} (x - x_j)(y - y_j)\phi_{a_j}(\mathbf{x} - \mathbf{x}_j)\Delta V_j = 0$$

$$\tilde{m}_{02} = \sum_{j=1}^{np} (y - y_j)^2\phi_{a_j}(\mathbf{x} - \mathbf{x}_j)\Delta V_j = 0 \ .$$

As in the one dimensional case, the approximations associated with Γ_g can be defined in a limiting sense. Conditions for which a 1D RKPM shape function calculation can be used along a boundary are derived for the particle distribution shown in Fig. 14. While the following example of degeneration is for three particles, the principles can be easily extended for other particle distributions.

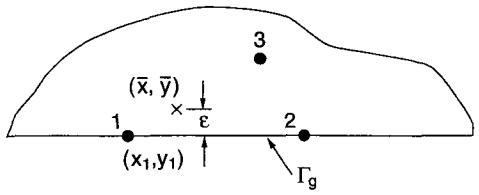

Fig. 14. Particle distribution demonstrating degeneration along a straight essential boundary

The shape function associated with particle 1 in Fig. 14 is evaluated in $(\bar{x}, \bar{y})$, where $\bar{y}$ is a distance ε from the boundary and $\bar{x}$ is arbitrary. As ε approaches zero, it will be shown the 2D shape function calculation degenerates into a 1D calculation along the boundary.

As seen from the 2D RKPM shape function definition for particle 1 at $\bar{\mathbf{x}}$

$$\begin{aligned} N_1(\bar{\mathbf{x}}) &= C(\bar{\mathbf{x}}; \bar{\mathbf{x}} - \mathbf{x}_1)\phi_{a_1}(\bar{\mathbf{x}} - \mathbf{x}_1)\Delta V_1 \\ &= \{b_{00}(\mathbf{a}, \bar{\mathbf{x}}) + b_{10}(\mathbf{a}, \bar{\mathbf{x}})(\bar{x} - x_1) \\ &\quad + b_{01}(\mathbf{a}, \bar{\mathbf{x}})(\bar{y} - y_1)\}\phi_{a_1}(\bar{\mathbf{x}} - \mathbf{x}_1)\Delta V_1 \ , \end{aligned} \tag{5.28}$$

the correction coefficients can be expressed in terms of the discrete moments,

$$b_{00} = \frac{\tilde{m}_{20}\tilde{m}_{02} - \tilde{m}_{11}^2}{\tilde{m}_{00}\tilde{m}_{20}\tilde{m}_{02} + 2\tilde{m}_{10}\tilde{m}_{01}\tilde{m}_{11} - \tilde{m}_{00}\tilde{m}_{11}^2 - \tilde{m}_{20}\tilde{m}_{01}^2 - \tilde{m}_{02}\tilde{m}_{10}^2} \tag{5.29a}$$

$$b_{10} = \frac{-\tilde{m}_{11}\tilde{m}_{01} + \tilde{m}_{10}\tilde{m}_{02}}{\tilde{m}_{00}\tilde{m}_{20}\tilde{m}_{02} + 2\tilde{m}_{10}\tilde{m}_{01}\tilde{m}_{11} - \tilde{m}_{00}\tilde{m}_{11}^2 - \tilde{m}_{20}\tilde{m}_{01}^2 - \tilde{m}_{02}\tilde{m}_{10}^2} \tag{5.29b}$$

$$b_{01} = \frac{\tilde{m}_{10}\tilde{m}_{11} - \tilde{m}_{20}\tilde{m}_{01}}{\tilde{m}_{00}\tilde{m}_{20}\tilde{m}_{02} + 2\tilde{m}_{10}\tilde{m}_{01}\tilde{m}_{11} - \tilde{m}_{00}\tilde{m}_{11}^2 - \tilde{m}_{20}\tilde{m}_{01}^2 - \tilde{m}_{02}\tilde{m}_{10}^2}. \tag{5.29c}$$

Evaluating the discrete moments for the particle distribution of Fig. 14 gives

$$\begin{aligned} \tilde{m}_{00} &= \phi_x(\bar{x} - x_1)\phi_y(\varepsilon)\Delta x_1\Delta y_1 + \phi_x(\bar{x} - x_2) \\ &\quad \times \phi_y(\varepsilon)\Delta x_2\Delta y_2 + \phi_x(\bar{x} - x_3)\varepsilon\Delta x_3\Delta y_3 \\ \tilde{m}_{10} &= (\bar{x} - x_1)\phi_x(\bar{x} - x_1)\phi_y(\varepsilon)\Delta x_1\Delta y_1 \\ &\quad + (\bar{x} - x_2)\phi_x(\bar{x} - x_2)\phi_y(\varepsilon)\Delta x_2\Delta y_2 \\ &\quad + (\bar{x} - x_3)\phi_x(\bar{x} - x_3)\varepsilon\Delta x_3\Delta y_3 \\ \tilde{m}_{01} &= \varepsilon\phi_x(\bar{x} - x_1)\phi_y(\varepsilon)\Delta x_1\Delta y_1 \\ &\quad + \varepsilon\phi_x(\bar{x} - x_2)\phi_y(\varepsilon)\Delta x_2\Delta y_2 \\ &\quad + \varepsilon\phi_x(\bar{x} - x_3)\varepsilon\Delta x_3\Delta y_3 \\ \tilde{m}_{11} &= (\bar{x} - x_1)\varepsilon\phi_x(\bar{x} - x_1)\phi_y(\varepsilon)\Delta x_1\Delta y_1 \\ &\quad + (\bar{x} - x_2)\varepsilon\phi_x(\bar{x} - x_2)\phi_y(\varepsilon)\Delta x_2\Delta y_2 \\ &\quad + (\bar{x} - x_3)\varepsilon\phi_x(\bar{x} - x_3)\varepsilon\Delta x_3\Delta y_3 \\ \tilde{m}_{20} &= (\bar{x} - x_1)^2\phi_x(\bar{x} - x_1)\phi_y(\varepsilon)\Delta x_1\Delta y_1 \\ &\quad + (\bar{x} - x_2)^2\phi_x(\bar{x} - x_2)\phi_y(\varepsilon)\Delta x_2\Delta y_2 \\ &\quad + (\bar{x} - x_3)^2\phi_x(\bar{x} - x_3)\varepsilon\Delta x_3\Delta y_3 \\ \tilde{m}_{02} &= \varepsilon^2\phi_x(\bar{x} - x_1)\phi_y(\varepsilon)\Delta x_1\Delta y_1 \\ &\quad + \varepsilon^2\phi_x(\bar{x} - x_2)\phi_y(\varepsilon)\Delta x_2\Delta y_2 \\ &\quad + \varepsilon^2\phi_x(\bar{x} - x_3)\varepsilon\Delta x_3\Delta y_3 \end{aligned} \tag{5.30}$$

where $(\bar{y}-y_1)$ and $(\bar{y}-y_2)=\varepsilon$, and $\phi_y(\bar{y}-y_3)\cong\varepsilon$ by definition.

In the limit as ε goes to zero, the $b_{01}(\bar{y}-y_1)$ term in Eq. (5.28) will drop out leaving b_{00} and $b_{10}(\bar{x}-x_1)$. Taking the limit of the above moments (Eq. 5.30) yields the following nonzero moments

$$\begin{aligned}\tilde{m}_{00} &= \phi_y(\varepsilon)\Delta y\{\phi_x(\bar{x}-x_1)\Delta x_1+\phi_x(\bar{x}-x_2)\Delta x_2\}\\ &= \phi_y(\varepsilon)\Delta y\tilde{m}_0\\ \tilde{m}_{10} &= \phi_y(\varepsilon)\Delta y\{(\bar{x}-x_1)\phi_x(\bar{x}-x_1)\Delta x_1\\ &\quad +(\bar{x}-x_2)\phi_x(\bar{x}-x_2)\Delta x_2\}\\ &= \phi_y(\varepsilon)\Delta y\tilde{m}_1\end{aligned}$$

$$\begin{aligned}\tilde{m}_{20} &= \phi_y(\varepsilon)\Delta y\{(\bar{x}-x_1)^2\phi_x(\bar{x}-x_1)\Delta x_1\\ &\quad +(\bar{x}-x_2)^2\phi_x(\bar{x}-x_2)\Delta x_2\}\\ &= \phi_y(\varepsilon)\Delta y\tilde{m}_2\ ,\end{aligned}\tag{5.31}$$

where it has been assumed that $\Delta y_1=\Delta y_2=\Delta y$, and $\tilde{m}_0,\tilde{m}_1$, and $\tilde{m}_2$ are one dimensional moment calculations for particles 1 and 2.

By inspection, the second term in the numerators of Eqs. (5.29b) and (5.29c) will vanish as ε goes to zero, leaving

$$b_{00}=\frac{\tilde{m}_{20}}{\tilde{m}_{00}\tilde{m}_{20}+\frac{2\tilde{m}_{10}\tilde{m}_{01}\tilde{m}_{11}}{\tilde{m}_{02}}-\frac{\tilde{m}_{00}\tilde{m}_{11}^2}{\tilde{m}_{02}}-\tilde{m}_{10}^2-\frac{\tilde{m}_{10}\tilde{m}_{02}^2}{\tilde{m}_{02}}}\tag{5.32a}$$

$$b_{10}=\frac{-\tilde{m}_{10}}{\tilde{m}_{00}\tilde{m}_{20}+\frac{2\tilde{m}_{10}\tilde{m}_{01}\tilde{m}_{11}}{\tilde{m}_{02}}-\frac{\tilde{m}_{00}\tilde{m}_{11}^2}{\tilde{m}_{02}}-\tilde{m}_{10}^2-\frac{\tilde{m}_{10}\tilde{m}_{02}^2}{\tilde{m}_{02}}}\tag{5.32b}$$

where both the numerator and denominator have been divided through by $\tilde{m}_{02}$.

The following expressions result from taking the limits of Eqs. 5.32b,

$$\begin{aligned}b_{00} &= \frac{\tilde{m}_{20}}{\tilde{m}_{00}\tilde{m}_{20}-\tilde{m}_{10}^2}=\frac{\tilde{m}_2}{(\tilde{m}_0\tilde{m}_2-\tilde{m}_1^2)\phi(0)\Delta y}\\ &= \frac{b_0}{\phi(0)\Delta y}\end{aligned}\tag{5.33a}$$

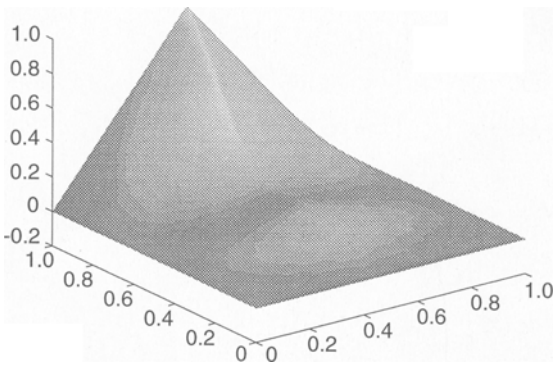

Fig. 15. Kronecker delta RKPM shape function along straight essential boundary

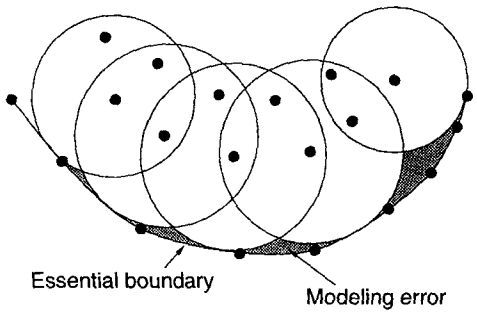

Fig. 16. Modeling error caused by using circular window supports near essential boundaries. By using conforming shape functions, the error can be avoided

$$\begin{aligned}b_{10} &= \frac{-\tilde{m}_{10}}{\tilde{m}_{00}\tilde{m}_{20}-\tilde{m}_{10}^2}=\frac{-\tilde{m}_1}{(\tilde{m}_0\tilde{m}_2-\tilde{m}_1^2)\phi(0)\Delta y}\\ &= \frac{b_1}{\phi(0)\Delta y}\ ,\end{aligned}\tag{5.33b}$$

in which b_0 and b_1 are 1D correction coefficients.

By substituting Eqs. (5.33) into Eq. (5.28), $N_1(\bar{\mathbf{x}})$ is defined in the limit as

$$\begin{aligned}N_1(\bar{\mathbf{x}}) &= \lim_{\varepsilon\to 0}\{b_{00}+b_{10}(\bar{x}-x_1)\\ &\quad +b_{01}(\varepsilon)\}\phi_x(\bar{x}-x_1)\phi_y(\varepsilon)\Delta x_1\Delta y_1\\ &= \left\{\frac{b_0+b_1(\bar{x}-x_1)}{\phi_y(0)\Delta y_1}\right\}\\ &\quad \times\phi_x(\bar{x}-x_1)\phi_y(0)\Delta x_1\Delta y_1\\ &= \{b_0+b_1(\bar{x}-x_1)\}\phi_x(\bar{x}-x_1)\Delta x_1\ .\end{aligned}\tag{5.34}$$

This is clearly a one dimensional calculation.

An interesting choice of linear basis shape functions for a straight essential boundary would be to use a dilation parallel to the boundary that corresponded FEM hat functions (Liu, Chen, Uras, and Chang, 1996). This shape function would satisfy the Kronecker delta condition at the boundary allowing the nodal values to be simply prescribed on the global equations. Such a shape function is depicted in Fig. 15.

In the case of curved boundaries, the typical approach is to approximate the boundary with piecewise polynomials. Given an admissible particle distribution, circular or oval shape functions can be generated with constant dilations that ensure that the interior shape functions vanish at the essential boundary. However, one should be aware that this procedure could introduce modeling error near the boundary. As seen in Fig. 16 a collection of admissible shape functions can fail to accurately represent a particular boundary. The shaded regions in the figure represent areas within the domain where there are no free interpolants associated with v^h.

By incorporating the dilation function, shape functions can be made to conform to the boundary thus removing areas of poor interpolation. Note that the dilation function is only necessary for shape functions in the proximity of the essential boundary. Following this method, an admissible particle distribution can be generated and dila-

tion coefficents for the dilation function can be defined using the geometry of the boundary.

6
Numerical examples

6.1
Helmholtz equation

To compare the accuracy of the various one dimensional techniques described in Section 5, the following Helmholtz equation is studied

$$u_{,xx}(x) + u(x) = 0 \ , \qquad 0 < x < 10 \tag{6.1a}$$

$$u(0) = 0 \tag{6.1b}$$

$$u(10) = 1 \tag{6.1c}$$

where the exact solution is given by

$$u(x) = \frac{\sin(x)}{\sin(10)} \ . \tag{6.2}$$

A cubic spline window and four point Gaussian quadrature was used with uniform particle distributions of 11, 22, 44, and 88 particles. Four methods of enforcing the essential boundary conditions were considered:

1. Lagrange multipliers (constant dilation of $1.17\Delta x$)
2. $C(x; x - x_j) = 0$ (interior dilation of $a = 1.17\Delta x$ and dilation of Δx near the boundaries)
3. $\phi(x - x_j) = 0$ (interior dilation of $1.17\Delta x$ and reduced constant dilations near boundaries)
4. $\phi(x - x_j) = 0$ (interior dilation of $1.17\Delta x$ and reduced linear dilation functions near boundaries)

The L_2 and H_1 error norms defined by

$$L_2 = \| \ (u^h - u^{exact}) \ \| = \left\{ \int_\Omega (u^h - u^{exact})^2 d\Omega \right\}^{1/2} \tag{6.3}$$

$$H_1 = \| \ (u^h_{,x} - u^{exact}_{,x}) \ \| = \left\{ \int_\Omega (u^h_{,x} - u^{exact}_{,x})^2 d\Omega \right\}^{1/2} \tag{6.4}$$

were used to measure the accuracy of the various methods. Figure 17 shows that the Lagrange multiplier technique gave the lowest error by the method of forcing the correction function to zero gives comparable accuracy with a higher convergence rate. In avoiding the inconveniences of Lagrange multipliers, the method in which the correction function equals zero at the boundary seems very attractive. The methods in which the window function was forced to zero suffered in accuracy, but for fine meshes the error was of the same order of magnitude for all the methods. It is evident that the error near the boundary dominates the convergence.

In comparing the constant and linear dilation methods used in forcing the window function to zero at the boundaries, it is apparent that the linear dilation yields a better solution for coarse grids, but does not perform as well for fine grids. The improved accuracy for coarse grids using the linear dilation function is a result of smoother shape functions as shown in Section 5. The shift in accuracy between the two methods for fine grids cannot be explained at this time.

6.2
Cantilever beam

The displacement given by Timoshenko and Goodier (Timoshenko and Goodier, 1970) for a unit width cantilever beam loaded at the end for plane stress (Fig. 18) are

$$u_x = \frac{-Py}{6EI}\left((6L - 3x)x + (2 + v)(y^2 - \frac{D^3}{4}) \right) \tag{6.5a}$$

$$u_y = \frac{P}{6EI}\left(3vy^2(L - x) + (4 + 5v)\frac{D^2 x}{4} + (3L - x)x^2 \right) \ . \tag{6.5b}$$

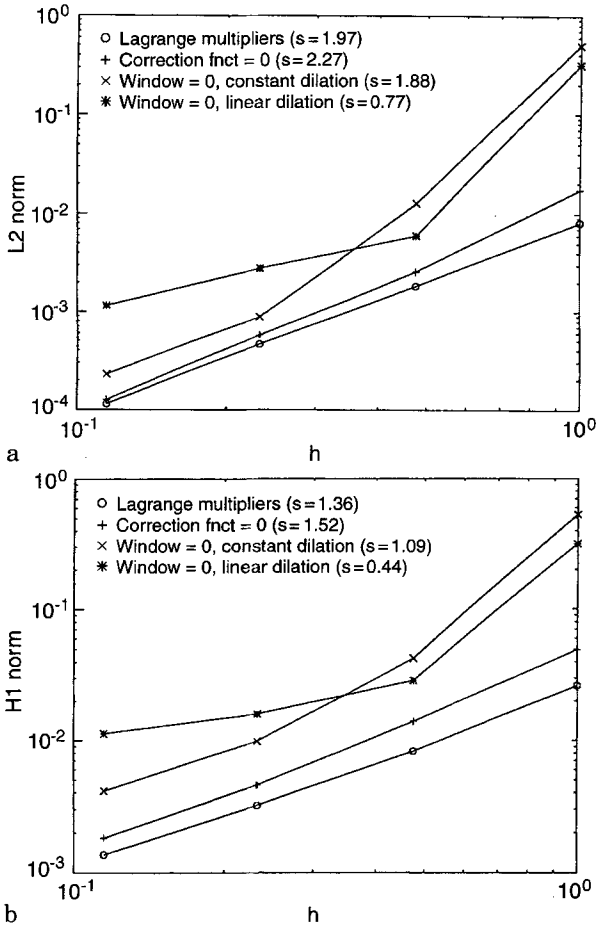

Fig. 17. a,b. L2 and H1 convergence of essential boundary techniques of one dimensional Helmholtz equation normalized by the norms of the exact solution. (a) L2 norm. (b) H1 norm

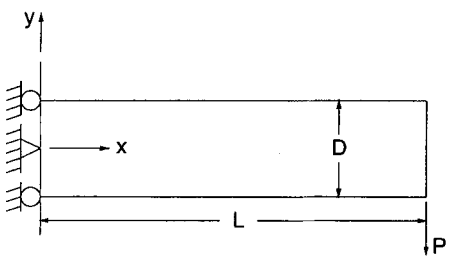

Fig. 18. Cantilever beam

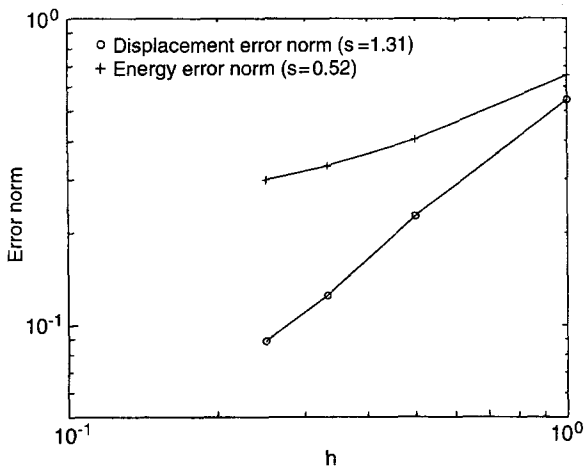

Fig. 19. Cantilever beam displacement error norm and energy error norm

The stresses are then

$$\sigma_{xx} = \frac{P(L-x)y}{I}$$
$$\sigma_{xy} = 0 \qquad (6.6c)$$
$$\sigma_{yy} = \frac{P}{2I}\left(\frac{D^2}{4} - y^2\right) ,$$

where I is the moment of inertia of the rectangular cross-section.

To reproduce the above solution, the essential boundary condition at $x = 0$, was imposed using Eqs. (6.5a) and the traction boundary condition at $x = L$ was distributed with a parabolicly according to Eq. (6.6c). The following material properties were used: $E = 1000$, $v = 0.3$, $L = 8$ and $D = 1$ with a unit load, P (Krongauz and Belytschko, 1996). A linear basis and a cubic spline window were used for the approximates and 4×4 Gauss quadrature was used for the integration.

To quantify the numerical accuracy of the methods, a L_2 displacement error norm and an energy error norm were used.

$$\|E\|_2 = \left\{ \int_\Omega (\mathbf{u}^h - \mathbf{u}^{exact})^T (\mathbf{u}^h - \mathbf{u}^{exact}) d\Omega \right\}^{1/2} \qquad (6.7)$$

$$\|E\|_e = \left\{ \int_\Omega \frac{1}{2} (\epsilon^h - \epsilon^{exact})^T (\sigma^h - \sigma^{exact}) d\Omega \right\}^{1/2} . \qquad (6.8)$$

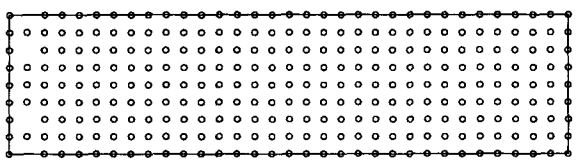

Fig. 20. Cantilever beam particle distribution with special distribution near essential boundary

Solutions were obtained for 18, 51, 100, and 165 nodes by forcing the window functions of nodes near the boundary to equal zero on the boundary. A dilation of $1.5\Delta x$ was used in both the x- and y-directions except for nodes near the boundary. The two rows of nodes closest to the boundary had dilations of $0.5\Delta x$ and Δx in the y-direction respectively. The convergence rates of the displacement norm and energy norm were 1.31 and 0.52 (Fig. 19).

The problem was also solved by forcing the correction function to equal zero on the boundary. A uniform grid of nodes was used except near the edges of the essential boundary. Near the edge, a distribution was used as shown in Fig. 20. Nine particles were used in the y-direction and 36 in the x-direction. With the two nodes removed near each edge, a total of 320 nodes were used.

Because a special node distribution was required near the essential boundary condition, the problem parameters were adjusted to allow for uniform grid spacings with a reasonable number of nodes. The following parameters were changed: $E = 3e7$, $L = 48$ and $D = 12$, $P = 40000$. A constant dilation of Δx was used.

The maximum analytic tip displacement under the above conditions is 0.356. The numerical solution yielded 0.353 giving an error of 0.843 percent.

7 Conclusions

A method of satisfying essential boundary conditions with meshless, admissible approximations has been introduced. The motivation for this development is to alleviate the burden of using Lagrange multipliers, modified variational principles, or other techniques for imposing essential boundary conditions that are not intuitive or result in undesirable global matrix configurations.

A dilation function, an extension of the RKPM dilation parameter, was also introduced. The advandage of a dilation function over a simpler definition, is its ability to allow shape functions near a boundary to conform to the geometry of the boundary thus reducing interpolation error. It was also shown that the dilation function can be used as a transition between shape functions with different dilations. In the case of the Helmholtz problem, it was evident that the incorporation of the dilation function reduced error for coarse grids when the window function was forced to zero on the boundary.

The admissible approximation technique, which satisfies the classical definition of the Galerkin method, can be achieved in two distinct ways; by forcing the correction function or the window function to equal zero at the boundary. In two dimensions, it was shown that near the boundary restrictions on the particle distribution, window and dilation were required to force the correction function to equal zero. In forcing the window function to zero, special care was needed to define approximations associated with the boundary to account for degeneration in certain geometries.

The Helmholtz equation studied in one dimension demonstrated that both techniques of generating admissible shape functions can achieve sufficient accuracy for two-point boundary value problems. The method of forcing the

correction function to zero was particularly promising. The cantilever beam problem however, showed that much is yet not fully understood in this technique. The convergence rates for forcing the window function to zero were not acceptable and prompt the question of what led to the error. At this time, it is believed that the moment matrix conditioning degrades near the essential boundary condition as a result of the degeneration of the shape function calculations.

Future areas of research should be concentrated in characterizing the behavior of the irregular shape functions produced by forcing the window function to zero near boundaries. Another area that needs development is extending the method of forcing the correction function to zero at boundaries of various geometries

References

Beissel, S.; Belytschko, T. (1996): Nodal integration of the element-free Galerkin method. To appear in Computer Methods in Applied Mechanics and Engineering

Belytschko, T.; Krongauz, Y.; Fleming, M.; Organ, D.; Liu, W. K. (1996): Smoothing and accelerated computations in the element-free Galerkin method. To appear in Journal of Computational and Applied Mathematics

Belytschko, T.; Lu, Y. Y.; Gu, L. (1994): Element-free Galerkin methods. Int. Num. Methods in Engineering 37: 229–256

Duarte, C. A.; Oden, J. T. (1995): Hp clouds – a meshless method to solve boundary-value problems. Technical Report 95–05, Texas Institute for Computational and Applied Mathematics, University of Texas at Austin

Hughes, T. J. R. (1987): The Finite Element Method. Englewood Cliffs, N.J.: Prentice-Hall.

Krongauz, Y.; Belytschko, T. (1996): Enforcement of essential boundary conditions in meshless approximations using finite elements. To appear in Computer Methods in Applied Mechanics and Engineering

Lancaster, P.; Salkauskas, K. (1981): Surfaces generated by moving least squares methods. Mathematics of Computation 37: 141–158

Liu, W. K.; Chen, Y. (1995): Wavelet and multiple scale reproducing kernel methods. International Journal for Numerical Methods in Fluids 21: 901–931

Liu, W. K.; Chen, Y.; Chang, C. T.; Belytschko, T. (1996): Advances in multiple scale kernel particle methods. Computational Mechanics

Liu, W. K.; Chen, Y.; Jun, S.; Chen, J.; Belytschko, T.; Pan, C.; Uras, R. A.; Chang, C. T. (1996): Overview and applications of the reproducing kernel particle methods. Archives of Computational Methods in Engineering; State of the art reviews 3: 3–80

Liu, W. K.; Y. Chen, Y.; Uras, R. A. (1995): Enrichment of the finite element method with reproducing kernel particle method. Current Topics in Computational Mechanics, eds. Cory, J. F. Jr., Gordon, J. L., ASME PVP 305: 253–258

Liu, W. K.; Chen, Y.; Uras, R. A.; Chang, C. T. (1996): Generalized multiple scale reproducing kernel particle methods. To appear in a special issue, Meshless Methods, in Computer Methods in Applied Mechanics and Engineering

Liu, W. K.; Jun, S.; Li, S; Adee, J.; Belytschko, T. (1995): Reproducing kernel particle methods for structural dynamics. International Journal for Numerical Methods in Engineering 38: 1655–1679

Liu, W. K.; Jun, S.; Zhang, Y. F. (1995): Reproducing kernel particle methods. International Journal for Numerical Methods in Engineering 20: 1081–1106

Liu, W. K.; Li, S.; Belytschko, T. (1996): Moving least square kernel method, methodology and convergence. Accepted for publication in Computer Methods in Applied Mechanics and Engineering

Lu, Y. Y.; Belytschko, T.; Gu, L. (1994): A new implementation of the element free Galerkin method. Computer Methods in Applied Mechanics and Engineering 113: 397–414

Oñate, E.; Idelsohn, S.; Zienkiewicz, O. C.; Taylor, R. L.; Sacco, C. (1996): A stabilized finite point method for analysis of fluid mechanics problems. submitted

Timoshenko, S. P.; Goodier, J. N. (1970): Theory of Elasticity (Third ed.). New York: McGraw Hill.